

**TO: M. MARDENFELD, A. BROOKS, D. LOESSER, R. ELLIS, S. GERHARDT, J. MENARD**  
**FROM: M.L. REINKE**  
**SUBJECT: IMPACT OF FACETING ON HEAT FLUX TO THE OUTBOARD DIVERTOR PFCS**

*FINDING: The present structure of the outboard divertor (OBD) approximates an axisymmetric surface by joining multiple flat plates, creating a faceted surface. This leads to varying areas of enhanced and reduced heat flux across each of the 48 nominally similar structures. For plasmas in the range of those specified in the PFC Requirements document, this would lead to heat flux enhancements of greater than 2.0. The ‘fish-scale’ shaping of tiles to hide leading edges and fastener access holes cannot be used to reduce this and actually makes the effect worse. Shaping of the PFC surfaces to be more axisymmetric, like the IBDV or CSFW, or shaping of tiles and/or backing plates for small-cube type schemes would reduce the enhancement but also complicate the design. This analysis can be used to help determine if/how the OBD needs to be modified to create a ‘high heat flux’ handling surface.*

As shown in Section 11 of the Vacuum Vessel and In-Vessel Hardware SDD and Figure 1, the NSTX-U outboard divertor is composed of multiple (48) flat plates that are angled relative to horizontal by  $\theta_{surf} = 21.5^\circ$  by mounting to the upper and lower ‘BBQ rails’ shown in DB1014 and DB1043. This results in a surface that is non-axisymmetric, leading to a variation in the heat flux across the tile surface, reducing the nominally axisymmetric heat flux that can be deposited before reaching temperature or stress limits.

To first examine this effect, it helps to look at a geometrically limiting cases. For a horizontal flat plate divertor, faceting does not lead to any enhancement, while the effect is maximized for a vertical plate divertor, shown in Figure 2. The variation in the heat flux to the target is computed by looking at the variation of  $\hat{B} \cdot \hat{n}$ , the dot product of the magnetic field with the surface normal, derived in Appendix A.

$$\hat{B} \cdot \hat{n} = -\frac{\sin \theta_{surf}}{\sqrt{1 + b_{rat}^2}} \left[ \sin(\theta_{surf} + \theta_{pol}) \cos \phi - b_{rat} \sin \phi + \frac{\cos(\theta_{surf} + \theta_{pol})}{\tan \theta_{surf}} \right]$$

where  $b_{rat} = B_T/B_P$  and the angles,  $\theta_{surf}$ ,  $\theta_{pol}$  and  $\phi$  are defined in Figure 2. An enhancement factor will be discussed, defined as  $EF \equiv (\hat{B} \cdot \hat{n})/(\hat{B} \cdot \hat{n})_{\phi=0}$  which for  $\theta_{surf} \rightarrow \pi/2$  and  $\theta_{pol} \rightarrow 0$  reduces to  $EF = \cos \phi (1 - \tan \phi / \tan \alpha)$

Before plotting variations for the OBD it helps to look at some magnified cases, constructed geometrically, to illustrate some basic phenomenology. In Figure 3, a view from the top down for a case with 9 facets (thus  $\Delta\phi = 40^\circ$  toroidal

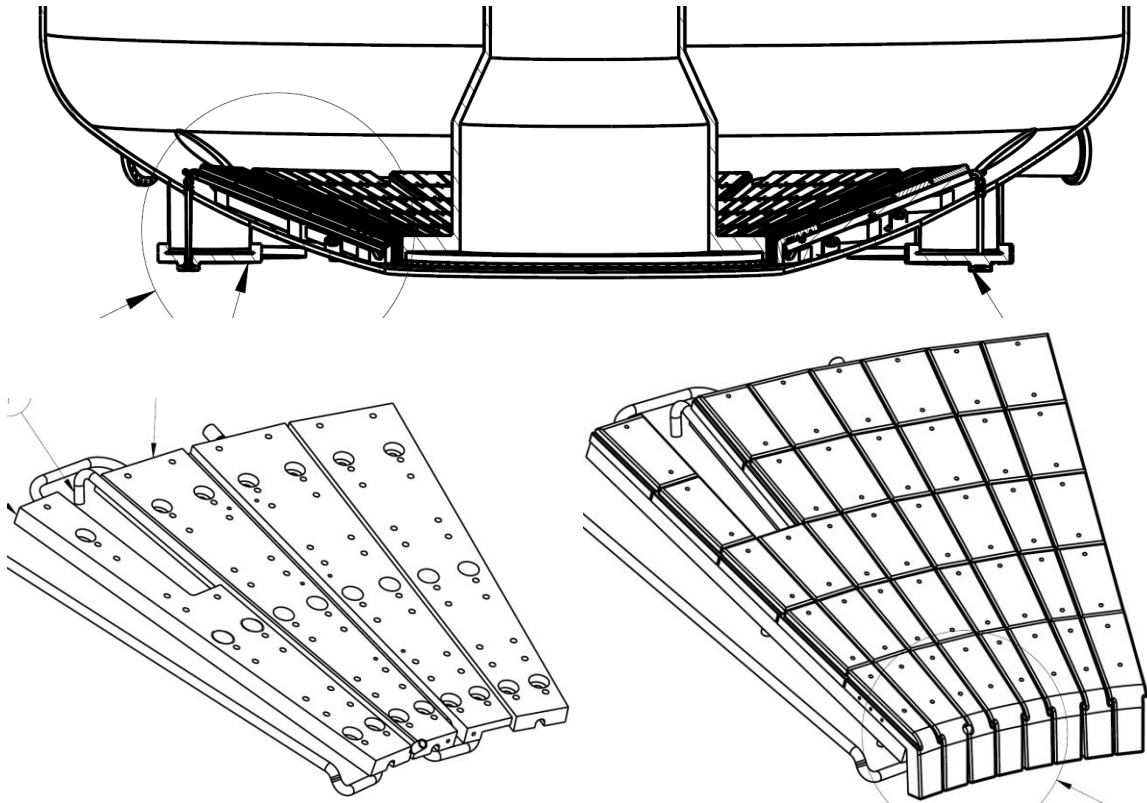


**Figure 1: Images from EA3010 showing the faceted and angled structure of the present NSTX-U outboard divertor**

segments) and a field line angle of  $\alpha = 15^\circ$  illustrates how the heat flux changes. At the center of the plate the heat flux is the same as for a perfectly conformal surface, but moving counter clockwise, towards the field line angle (in this case  $b_{rat} < 0$  since  $B_\phi$  is in the  $-\hat{\phi}$  direction), the angle between the plate and the field line increases, enhancing the heat flux. Moving clockwise, the opposite occurs and the heat flux is reduced. In cases like this shown where the facet toroidal angle,  $\Delta\phi$ , is such that  $\Delta\phi/2 > \alpha$ , then the field lines become tangent, miss the surface and a shadowed area develops. A shadowed area in the counter-clockwise direction also forms, but this requires a rather detailed calculation, and is shown in Appendix B.

It's also apparent from this figure that if one were to shape the tiles toroidally to hide leading edges, the strategy would be different depending on the expected range of field line angles. If  $\alpha < \Delta\phi/2$  over all operational space, then there is already no power going to the leading edges and in fact, it may be favorable to rotate the tiles *toward* the field (a rotation about the  $+z$ -axis) which could slightly reduce the faceting enhancement. If there is operational space where  $\alpha > \Delta\phi/2$  then the leading edges at the facet corners will be exposed and a rotation away from the field (a rotation about the  $-z$ -axis) would be necessary, further exacerbating the heat flux handling problem at small impact angles.

As shown in Figure 1, each of the 48 facets have two tiles, a larger ‘over’ and smaller ‘under’ tile, so variation of the heat flux will be shown that actually spans both tile surfaces, with the ‘under’ tile seeing higher heat flux than the ‘over’. The heat flux enhancement,  $EF$ , for the geometry of the NSTX-U outboard divertor is shown in Figure 4-Figure 6, for varying values of  $b_{rat}$  and  $\theta_{pol}$ . While it is not directly apparent in the  $\hat{B} \cdot \hat{n}$  equation, the dot product is not very sensitive to the sign of  $\theta_{pol}$  so the results shown are characteristic of a wide variety of poloidal impact angles.

For Figure 4,  $\theta_{pol} = 0$  results in  $\alpha = \tan(1/b_{rat})$ , which for  $b_{rat} = 15$  corresponds to  $\alpha = 3.8^\circ$  and  $b_{rat} = 55$  corresponds to  $\alpha = 1.05^\circ$ . As  $b_{rat}$  increases, the enhancement factor changes more strongly over the tile. For the nominally  $1^\circ$  angle of incidence cases that are characteristic of high poloidal flux expansion, there will be substantial change of heat flux over the tile in the toroidal direction. This increases as  $|\theta_{pol}| > 0$ .

For the particulars of the NSTX-U OBD geometry, there is some operational space for which shadowing due to the facet structure will occur (e.g.  $b_{rat} = 45, 55$  for  $\theta_{pol} = 20^\circ, 40^\circ$ ). This means that for smaller values of  $b_{rat}$  the leading edges will be exposed and to avoid this, a ‘fish-scale’ shaping could be used, due to the fixed helicity expected for OBD operations. As evident from Figure 3, a rotation to hide leading edges would worsen the enhancement due to the faceting and increase the shadowing for large  $b_{rat}$ . The quantitative extent of this could be investigated if necessary by furthering the method in Appendix A.

Presently the Recovery Project is considering various scenarios to improve heat flux handling for PFCs. For the OBD, there is the expectation that some toroidal variation in heat flux originates from the lack of axisymmetry in the ‘BBQ rails’ mounting structure. Even if this is fixed, the faceting effect discussed here will remain unless accounted for via shaping of the PFCs or mounting structures to better approximate a conical surface. This should be taken into account when considering the full scope of work necessary to make the OBD a ‘high heat flux’ handling structure, in contrast to simply restricting operations.



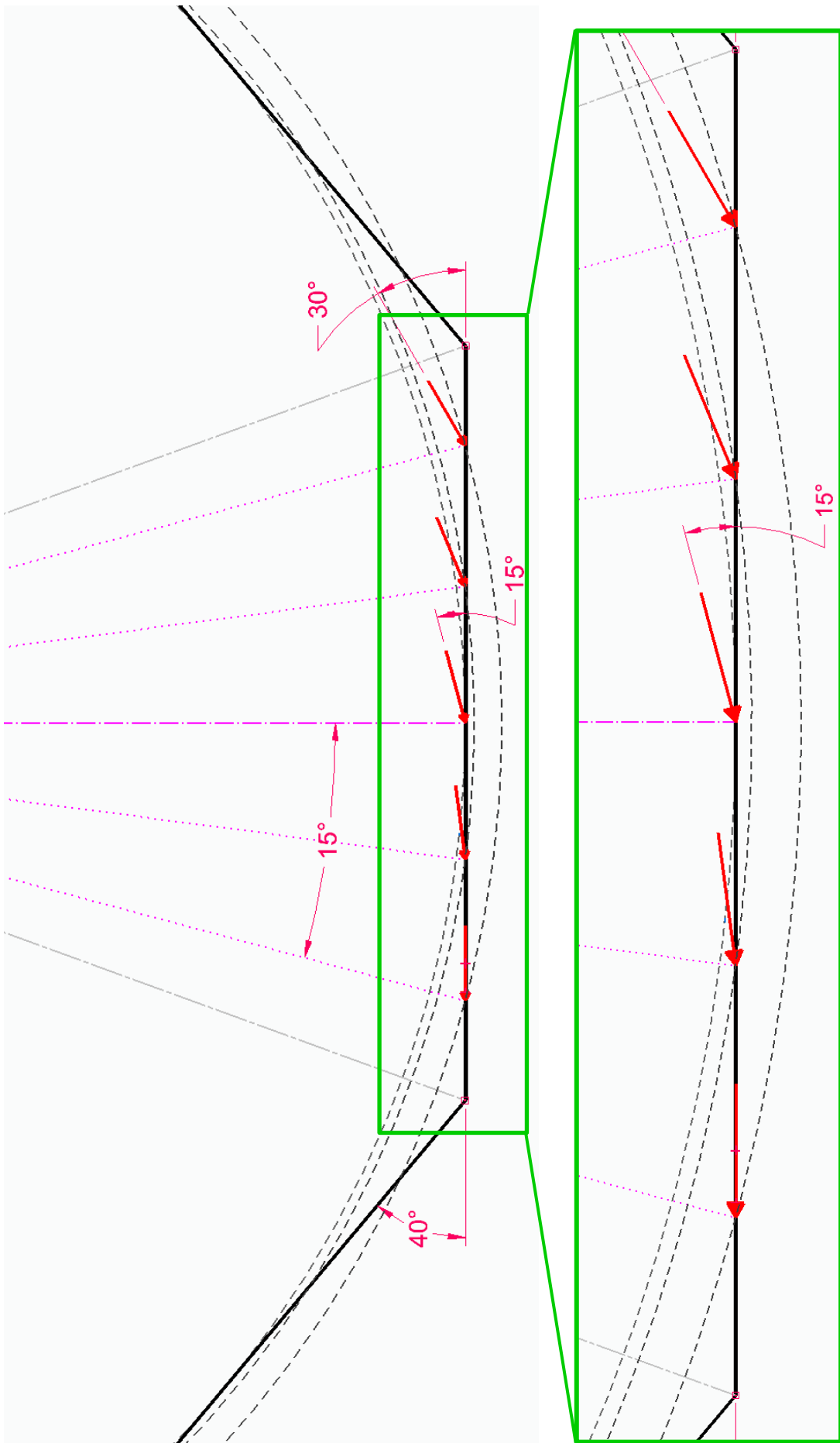


Figure 3: Exacerbated,  $n = 9$ , vertical plate faceted divertor with  $\alpha = 15^\circ$ , highlighting the how the impact angle changes across the facet and can become tangent, leading to shadowing.

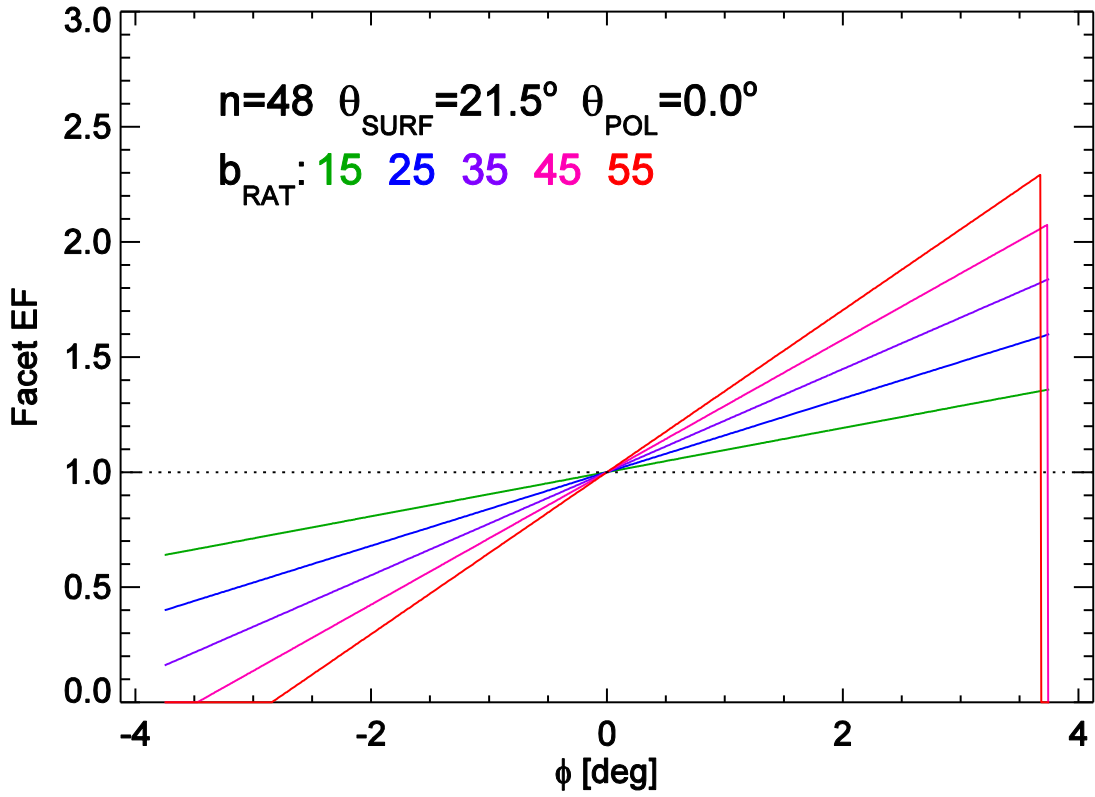


Figure 4: Enhancement for the NSTX-U OBD with  $\theta_{pol} = 0^\circ$ , and varying angles of incidence.

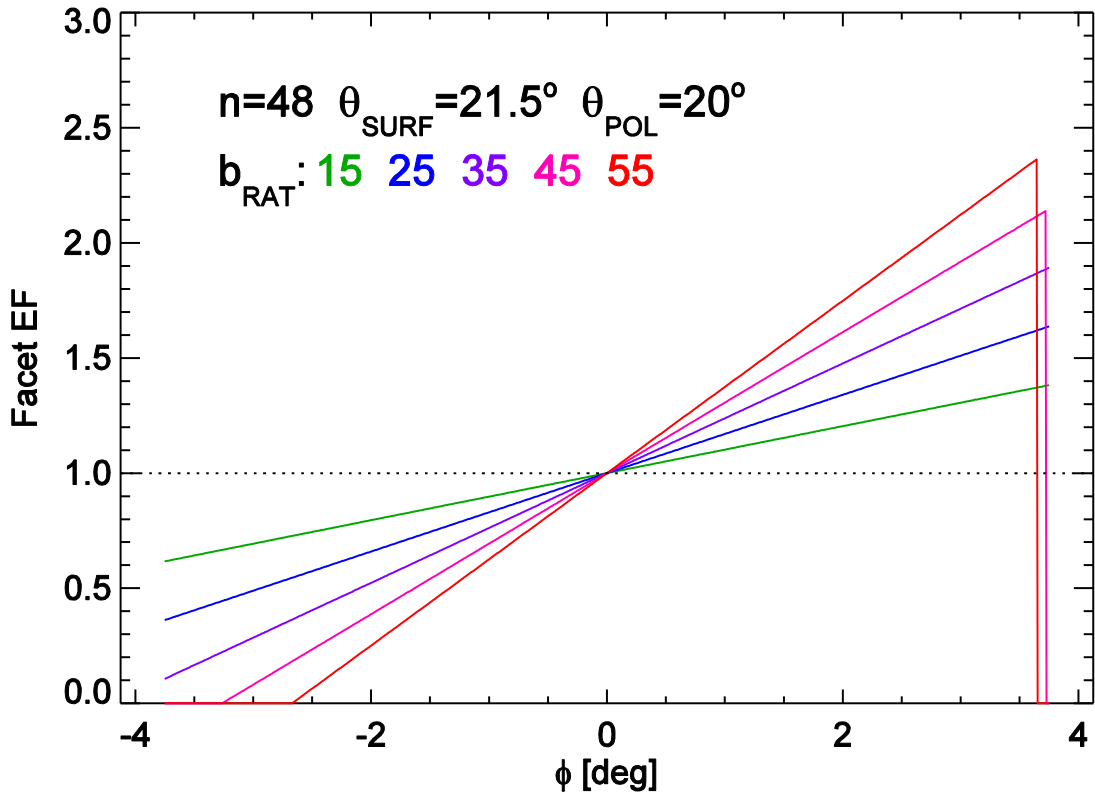


Figure 5: Enhancement for the NSTX-U OBD with  $\theta_{pol} = 20^\circ$ , and varying angles of incidence.

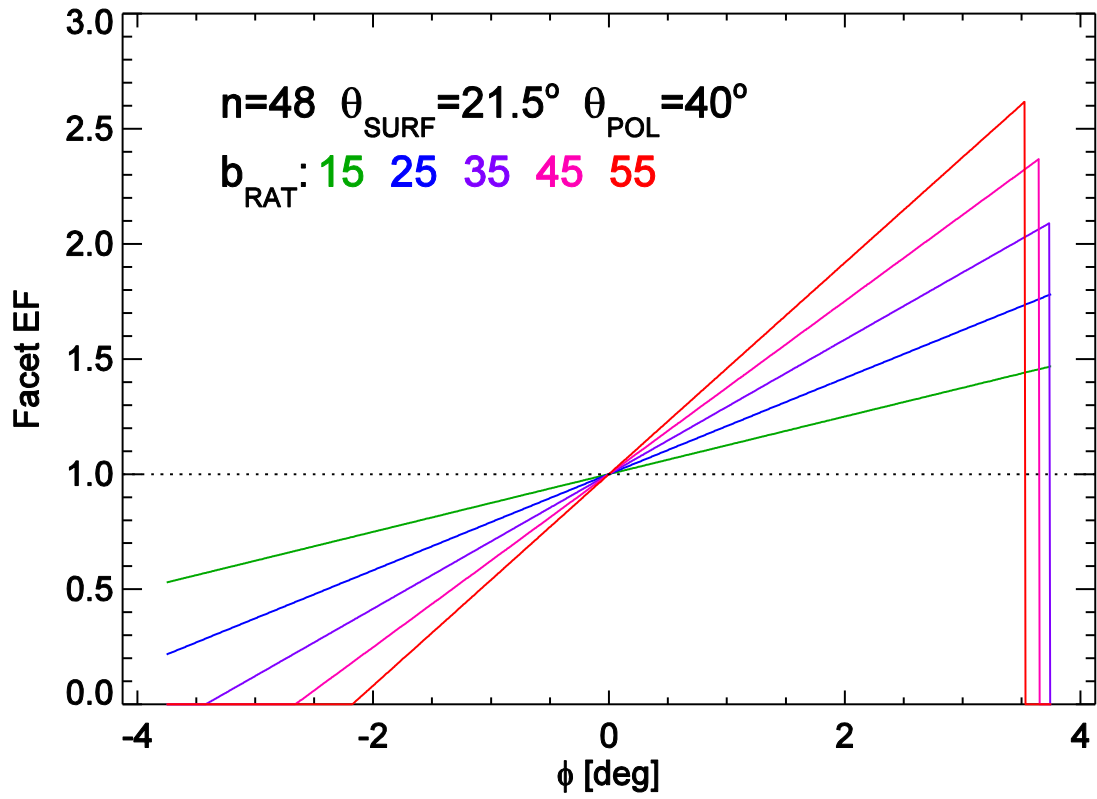


Figure 6: Enhancement for the NSTX-U OBD with  $\theta_{pol} = 40^\circ$ , and varying angles of incidence.

## APPENDIX A: Calculation of the Magnetic Field and Surface Normal Dot Product for a Faceted Surface

Computing  $\hat{B} \cdot \hat{n}$  is simply a matter of keeping track of coordinate systems and field and surface parameterizations. The axisymmetric magnetic field in a tokamak is

$$\vec{B} = \vec{B}_\phi + \vec{B}_p = F(\psi)\nabla\phi + \nabla\phi \times \nabla\psi$$

Where  $\nabla\phi = R\hat{\phi}$  and  $\psi = (1/2\pi) \int \vec{B}_p \cdot d\vec{A}$  is the poloidal flux function. The poloidal field can be further broken down into the radial field,  $B_R = -R^{-1} d\psi/dZ$  and vertical field,  $B_Z = R^{-1} d\psi/dR$ . The functions for  $F(\psi)$  and  $\psi(R, Z)$  are found using equilibrium codes when can forward model the expected fields from coil currents and assumptions about the plasma or attempt to infer these from experimental measurements. This is a standard forward and inverse problem that is solved throughout the community, so it can be assumed that the magnetic field unit vector,

$$\hat{B} = \frac{B_R}{B} \hat{R} + \frac{B_\phi}{B} \hat{\phi} + \frac{B_Z}{B} \hat{Z}$$

is known everywhere, with  $B^2 = B_\phi^2 + B_R^2 + B_Z^2$ . For non-conical surfaces, the radial and azimuthal unit vectors need to be converted, and we will use co-located Cartesian system that for  $\phi = 0$ , has  $\hat{R} = \hat{x}$  and  $\hat{\phi} = \hat{y}$ , which is the Front/Top/Right system in Figure 7, referred to as  $(xyz)_0$ . This allows the field unit vector to be expressed as

$$\hat{B} = B^{-1}[(B_R \cos \phi - B_\phi \sin \phi)\hat{x} + (B_R \sin \phi + B_\phi \cos \phi)\hat{y} + B_Z\hat{z}]$$

The faceted surface is a rotated and displaced plane, also shown in Figure 7 as Plane 11, referred to as  $(xyz)_1$ . For a single rotation of  $\theta_{surf}$  about  $\hat{y}_1$ ,  $\hat{z}_1$  is the surface normal which in the  $(xyz)_0$  coordinate system is

$$\hat{n} = -\sin \theta_{surf} \hat{x} + \cos \theta_{surf} \hat{z}$$

Note that a further rotation about  $\hat{x}_1$  would be used for things like fish-scaling or to study leading edges. Before combining, another change in parameterization is proposed, since in many cases, the radial and vertical field are generally not numbers that are not carried or listed in all analysis like in the tables for JEMv3. As shown in in Figure 2, the poloidal field is known (or designed to have) some misalignment with the surface normal,  $\theta_{pol}$  making

$$\begin{aligned} B_R &= B_p \sin(\theta_{surf} + \theta_{pol}) \\ B_Z &= -B_p \cos(\theta_{surf} + \theta_{pol}) \end{aligned}$$

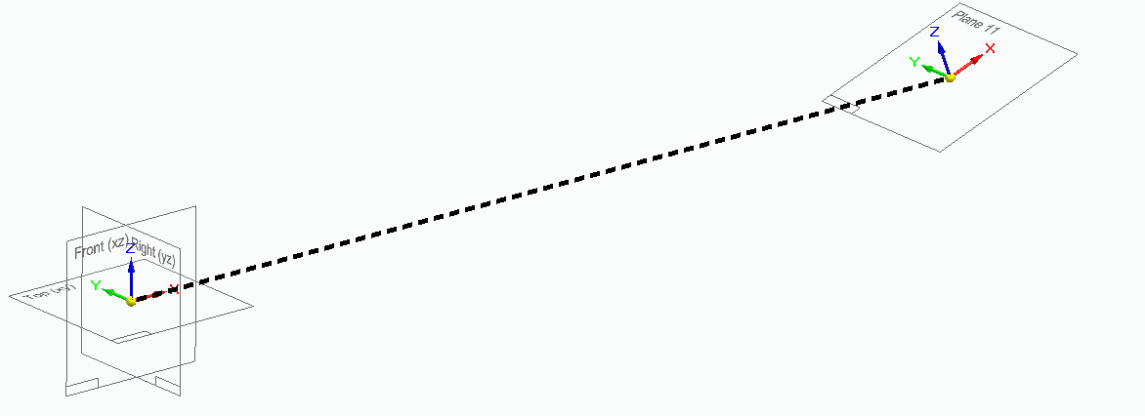


Figure 7: Layout of the facet coordinate system (Plane 11) from the center of the tokamak center.

Combining these and computing  $\hat{B} \cdot \hat{n}$  results in

$$\hat{B} \cdot \hat{n} = -\sin \theta_{surf} \left[ \frac{B_p}{B} \sin(\theta_{surf} + \theta_{pol}) \cos \phi - \frac{B_\phi}{B} \sin \phi \right] + \frac{B_p}{B} \cos \theta_{surf} \cos(\theta_{surf} + \theta_{pol})$$

In the limit of  $\theta_{surf} \rightarrow 0$  this reduces to  $\hat{B} \cdot \hat{n} = \frac{B_p}{B} \cos \theta_{pol}$  and there is no dependence on  $\phi$  as expected. In the limit of  $\theta_{surf} \rightarrow \pi/2$  the dot product becomes  $\hat{B} \cdot \hat{n} = -\left( \frac{B_p}{B} \cos \theta_{pol} \cos \phi - \frac{B_\phi}{B} \sin \phi \right)$ .

One further reduction (or complication) can be to replace the field ratios, defining  $b_{rat} = B_T/B_P$  where the field line angle,  $\alpha$ , for a horizontal plate ( $\theta_{surf} = 0$ ) with  $\theta_{pol} \rightarrow 0$  is  $\alpha = \text{atan } 1/b_{rat}$ . This makes the dot product

$$\hat{B} \cdot \hat{n} = -\frac{\sin \theta_{surf}}{\sqrt{1 + b_{rat}^2}} \left[ \sin(\theta_{surf} + \theta_{pol}) \cos \phi - b_{rat} \sin \phi + \frac{\cos(\theta_{surf} + \theta_{pol})}{\tan \theta_{surf}} \right]$$

and an enhancement factor is defined to be  $EF \equiv (\hat{B} \cdot \hat{n}) / (\hat{B} \cdot \hat{n})_{\phi=0}$  which for  $\theta_{surf} \rightarrow \pi/2$  and  $\theta_{pol} \rightarrow 0$  reduces to  $EF = \cos \phi (1 - \tan \phi / \tan \alpha)$ . Since we expect that  $\phi$  is relatively small for a reasonably designed divertor, the primary change in the heat flux is to linearly increase (and decrease) away from the center towards (away) from the direction of the field. This also foreshadows something strange happening when  $\phi > \alpha$ , which is discussed in Appendix B.

## APPENDIX B: Calculation of Shadowed Areas on a Faceted, Vertical Plate Divertor

As discussed in the main text, when toroidal angle of the facet becomes large relative to the angle of incidence from the plasma,  $\alpha$ , shadowed areas will develop on the tile. While the heat flux enhancement can be computed from the change of  $\hat{B} \cdot \hat{n}$ , its domain needs to be computed independently. In practice, this can be done by assuming regions on the tile beyond which the field lines become tangent, and then use power balance to calculate the other angle, but in this Appendix, for the case of the vertical plate divertor, a set of implicit equations can be solved which can be shown to be consistent with that approach.

### Power Balance

For a conformal surface, the power per unit height on the plate,  $P'_{cyl}$ , is

$$P'_{cyl} = n \int_{-\Delta\phi/2}^{+\Delta\phi/2} q_{\parallel} \sin \alpha R_o d\phi$$

where  $n$  is the number of facets and  $\Delta\phi = 2\pi/n$ . For the faceted plates of length  $\Delta l$ , the same amount of power,  $P'_{flat}$ , must be exhausted with

$$P'_{flat} = n \int_{-\Delta l/2}^{+\Delta l/2} q_{\parallel} \hat{B} \cdot \hat{n} dl$$

Setting the two equal to each other and converting the integral over  $dl$  to  $d\phi$

$$n q_{\parallel} \sin \alpha R_o \Delta\phi = n q_{\parallel} \int_{-\Delta\phi/2}^{+\Delta\phi/2} \frac{\hat{B} \cdot \hat{n}}{\cos^2 \phi} R_o d\phi$$

$$\Delta\phi = \int_{-\Delta\phi/2}^{+\Delta\phi/2} \frac{\hat{B} \cdot \hat{n}}{\sin \alpha \cos^2 \phi} d\phi$$

This gives an easy way to check and make sure the calculation has been done properly, as well as demonstrates a suitable enhancement factor to be defined,  $EF = \hat{B} \cdot \hat{n} / \sin \alpha$ .

### Enhancement Factor Limits

The equation for  $\hat{B} \cdot \hat{n}$  that is derived in Appendix A can be computed for an arbitrary range of  $\phi$ , but this does not indicate, directly, which areas are shadowed. On the  $EF < 1$  side of the facet, when  $\hat{B} \cdot \hat{n}$  crosses zero, the remaining region is shadowed. For  $EF > 1$ , either power balance or the following calculation can be used. This is derived for  $\theta_{surf} = 90^\circ$  and is shown to be consistent with power balance. For non-vertical, faceted divertors, a more

complicated analytical formalism is required, so power balance is recommended and is what is used in the main section of the memo for the NSTX-U outboard divertor.

In Figure 9 and Figure 10, the relevant triangles are highlighted for the  $n = 9$  faceted divertor with  $B_z = 0$  ( $\theta_{pol} = 0$ ) and  $\tan \alpha = B_R/B_\phi$  with  $\alpha = 15^\circ$ . The field line which just misses the facet to the right is constructed geometrically, by extrapolating a the field line to progressively larger circles, and re-adjusting the angle to be  $15^\circ$ . In practice this is a logarithmic spiral. There are two triangles which are used to find the the angle,  $\phi'$ , from center, after which the shadowed area begins on the  $EF > 1$  side of the facet. Equating the sum of the vertical distances gives

$$\frac{R_o}{\cos \alpha} \cos(\Delta\phi - \alpha) + l_2 \sin \Delta\phi = R' \cos \phi'$$

$$\frac{1}{\cos \alpha} \cos(\Delta\phi - \alpha) + \left( \tan \frac{\Delta\phi}{2} - \tan \alpha \right) \sin \Delta\phi = \frac{1}{\cos \alpha} e^{(\Delta\phi - \phi' - \alpha) \tan \alpha} \cos \phi'$$

If  $\alpha = \Delta\phi/2$  then the LHS reduces to 1 and the solution becomes  $\phi' = \Delta\phi/2$ , as expected. An approximate solution could be found, but its simply easier to numerically solve this relation. Energy balance can be used to confirm that the integration bounds move from  $-\frac{\Delta\phi}{2} < \phi < +\frac{\Delta\phi}{2}$  to  $-\alpha < \phi < \phi'$ .

In Figure 8, the heat flux enhancement is shown for a vertical plate divertor with  $n = 96$ , with a  $b_{rat}$  which correspond to  $\alpha = 5.7^\circ$  ( $b_{rat} = 10$ ) to  $\alpha = 0.95^\circ$  ( $b_{rat} = 60$ ). For large poloidal flux expansion, this effect is important and creates a large amount of shadowed area. For the ITER monoblock divertors,  $n \sim 1000$ , so the effect is much weaker. For Alcator C-Mod, the outer divertor has  $n = 120$ , but the tiles are machined to have a cylindrical front face, avoiding the enhancement.

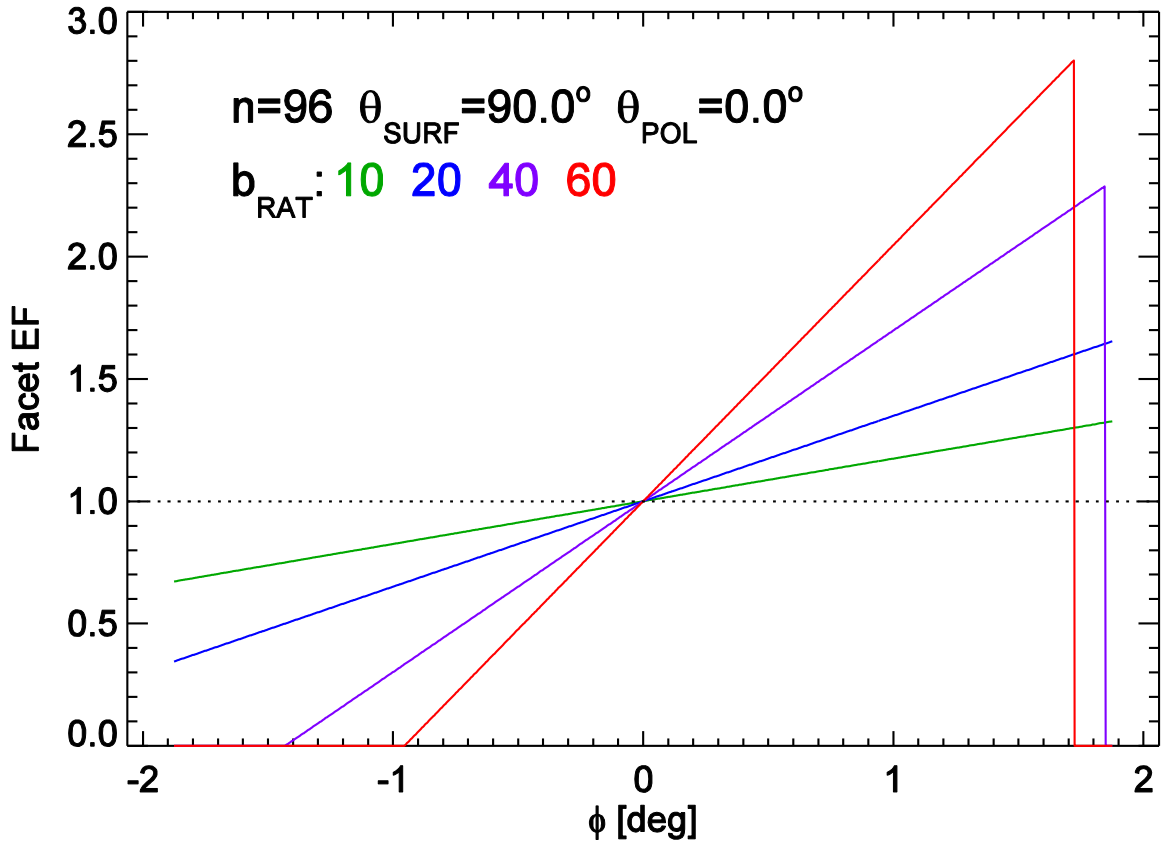


Figure 8: Calculation of heat flux enhancement factor,  $EF$ , for vertical plate, showing the shadowed regions for large values of  $b_{rat}$ .

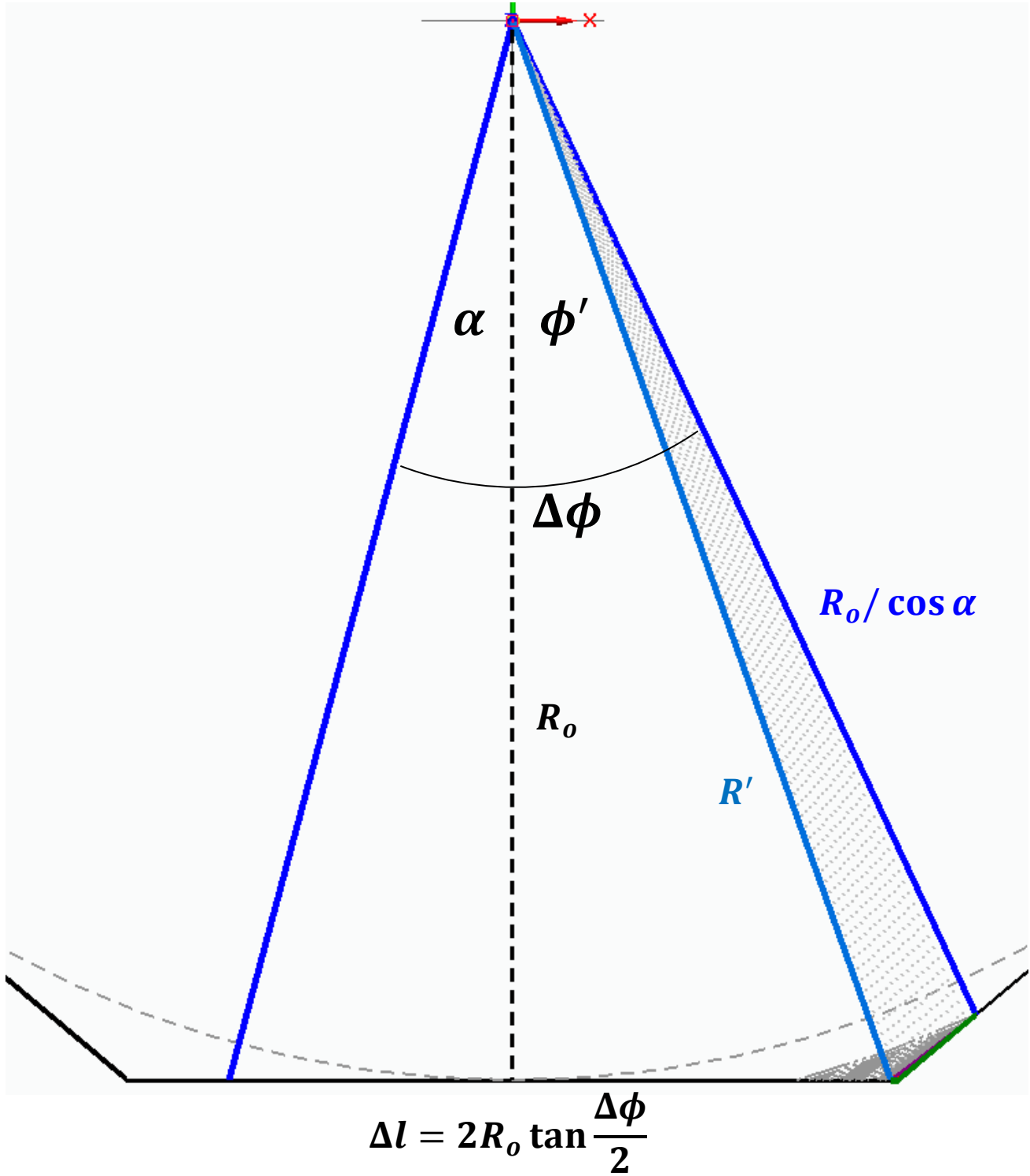


Figure 9: Top down view of faceted, vertical plate diverter for  $n = 9$  and  $\alpha = 15^\circ$  exacerbating the effect.

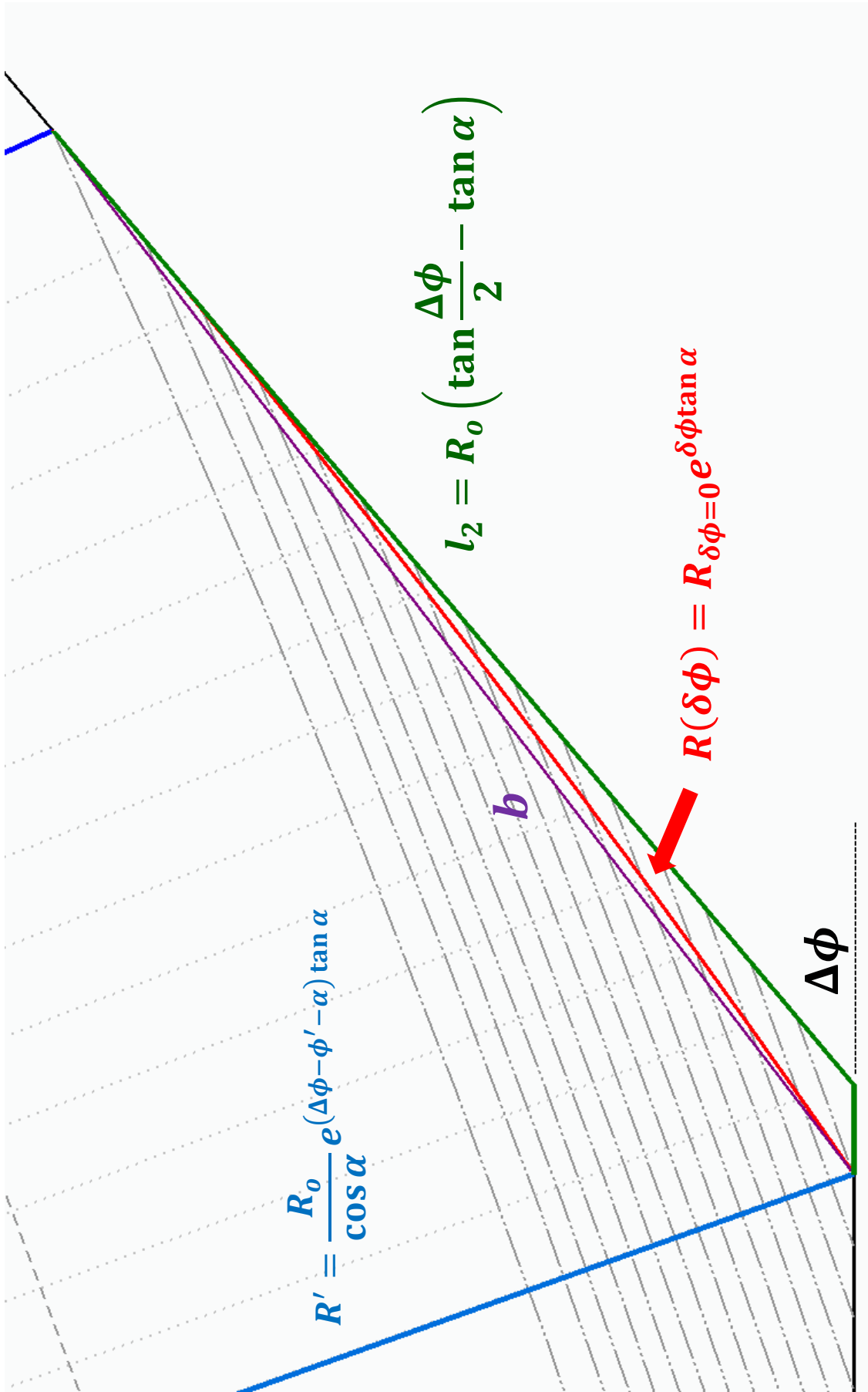


Figure 10: Zoom in of the setup shown in Figure 9 highlighting the shadowed region for  $EF > 1$

## Record of Changes

Rev.	Date	Description of Changes
0	6/12/2017	initial draft release to PFCR-WG
1	6/12/2017	Updated OBD to be $\theta_{surf} = 21.5$ and used $n = 48$ after discussions with Mardenfeld correctly indicated the over/under tiles are on the same facet.
2	6/26/2017	Changed distribution list to reflect PFC reorganization